Journal of Materials Chemistry A

Accepted Manuscript

Volume 4 | Number 1 | 7 January 2016 | Pages 1–330

Journal of
Materials Chemistry A

Materials for energy and sustainability
www.rsc.org/MaterialsA

ISSN 2050-7488

ROYAL SOCIETY OF CHEMISTRY

PAPER
Kun Chang, Zhaorong Chang et al
Bubble-template-assisted synthesis of hollow fullerene-like
MoS₂ nanocages as a lithium ion battery anode material

175 YEARS

ROYAL SOCIETY
OF CHEMISTRY

rsc.li/materials-a

ARTICLE

Post-synthesis deposition of mesoporous niobic acid with improved thermal stability by kinetically controlled sol-gel overcoating

Yuan-Peng Du[a], Florent Héroguel[a], Xuan Trung Nguyen[a] and Jeremy S. Luterbacher[a]*

Niobia is a well-known solid acid catalyst owing to its intrinsic Brønsted and Lewis acidity. However, catalyst development with this oxide has been limited by our ability to control its pore structure and thermal stability. Here we report a novel post-synthetic approach for preparing mesoporous niobia catalysts. This method relies on controlling the kinetics of niobium (V) ethoxide to deposit conformal Nb_2O_5 overcoats on SBA-15 in a typical Stöber solution. Full Nb_2O_5 coverage over the mesopores of SBA-15 was achieved by adding 4 monolayer equivalents of precursor ($4Nb_2O_5$@SBA-15), which was verified by X-Ray Photoelectron Spectroscopy. This overcoated SBA-15 had a high surface area and retained a narrow as well as ordered pore size distribution. Importantly, the typical structural transition from the amorphous to pseudo-hexagonal Nb_2O_5 phase did not occur with the overcoat after calcination at 773 K. Limiting this crystallization imparts an unprecedented thermal stability to our niobia overcoat, which enables the acid sites to be well preserved after catalyst regeneration. Furthermore, $4Nb_2O_5$@SBA-15 showed higher yields than commercial niobia (HY-340) and lab-synthesized bulk niobia in two probe reactions: xylose dehydration to furfural and Friedel-Crafts alkylation. In both cases, the improvement could be explained by the unique structural features of the niobia overcoat, including a favorable ratio of Brønsted and Lewis acid sites in the case of xylose dehydration and a high proportion of isolated Nb-OH groups for the alkylation reaction. Such structural features and unprecedented thermal stability provide additional tools for synthetizing unique solid acid catalysts using a simple post-synthesis deposition method.

Introduction

Niobium pentoxide (niobia) is a popular material in several catalytic and chemical applications including for use as sensing materials,[1–3] catalysts in biomass conversion,[4,5] electrochromic devices,[6] photocatalysts in oxidation,[7] and acid catalysis.[8–14] One of the reason for its popularity in catalysis is the acidic properties of niobium oxide, which have a high structural dependency.[15–17] Hydrated niobium pentoxide, usually denoted as $Nb_2O_5 \cdot H_2O$, is an amorphous solid and possesses strong Brønsted and Lewis acidity, while other more thermodynamically stable phases, including its pseudo-hexagonal (TT-phase) and monoclinic form, are less acidic and non-acidic, respectively.[15,16] Because solid acid catalysts are considered less corrosive and more environmentally benign than traditionally used homogeneous acids, interest in niobic acid-based catalysts has been increasing in the past decade. In this context, many synthesis methods

for producing niobia catalysts have been reported with a special focus on maximizing acidity and surface area including through template assisted approaches,[18–20] exfoliation[21] and hydrothermal processes.[11] The catalysts prepared by exfoliation and hydrothermal processes usually show strong acidities but lower surface areas (less than 200 $m^2 \cdot g^{-1}$). Mesoporous Nb_2O_5 with high surface areas can be obtained using a template assisted synthesis but its pore size distributions are typically broader (± 2 nm) than that of mesoporous silica (e.g. MCM-41 and SBA-15). Recently, a novel post-synthesis method was reported where Nb_2O_5 was overcoated on SBA-15 by atomic layer deposition (ALD) and this overcoated SBA-15 had both a narrow pore size distribution (± 1 nm) as well as a high surface area.[22] Nevertheless, the high cost of ALD instrumentation and coating processes motivates the development of simpler and more affordable liquid-phase strategies that are much more compatible with large scale catalyst synthesis. Additionally, the activity for acid catalysis using overcoated SBA-15 was not fully investigated. We recently reported a simple and scalable sol-gel based approach for overcoating Al_2O_3 on SBA-15. This approach relied on slowing down the condensation rate of Al(sec-BuO)$_3$ by adding ethyl acetoacetate (EAA) and

a. Laboratory of Sustainable and Catalytic Processing, Institute of Chemical Sciences and Engineering, École Polytechnique Fédérale de Lausanne (EPFL), CH-1015 Lausanne, Switzerland.

ARTICLE

Journal Name

maintaining a low precursor concentration in the reaction media using a syringe pump setup.[23] Here, we extend this kinetic control strategy to the niobia sol-gel system and develop a new post-synthesis method to prepare a SBA-15 type mesoporous niobia as a solid acid catalyst. Thanks to its unique structural features and acidity, this overcoated catalyst is highly active for both xylose dehydration and Friedel-crafts alkylation and has an unprecedented thermal stability against acidity loss, which commonly occurs due to structural reorganization.

Experimental section

Chemicals and Materials

All chemicals used in this study were analytical grade and obtained from commercial suppliers. They were used without further purification unless stated otherwise. Air and moisture-sensitive reagents were handled using a nitrogen filled glove box or a standard Schlenk line apparatus. Xylose, anisole, and benzyl alcohol, Pluronic 123 (P123), ethyl acetoacetate and decane were purchased from Sigma Aldrich. Tetraethyl orthosilicate (TEOS), 2-furaldehyde (furfural) and tetramethyl orthosilicate (TMOS) were purchased from Acros. $HCl_{(aq)}$ (ca. 37%) was purchased from Merck. Ethanol was purchased from Fisher Scientific. Niobium (V) ethoxide ($Nb(OEt)_5$) was purchased from ABCR. $NH_{3(aq)}$ (ca. 25%) and toluene were purchased from VWR Chemicals. Dioxane was purchased from Roth. Hydrated niobium oxide ($Nb_2O_5 \cdot nH_2O$, HY-340) was provided free of charge by Companhia Brasileira de Metalurgia e Mineração (CBMM). Furfural and EAA were purified by distillation under reduced pressure prior to being used. The water used in this study was purified by a Millipore Milli-Q Advantage A10 water purification system resulting in a resistivity higher than 18 MΩ·cm. All gases were purchased from Carbagas.

Catalyst characterization

Physisorption was conducted on a Micromeritics 3 Flex instrument. The samples were dried under reduced pressure at 423 K prior to N_2 adsorption. The specific surface area (S_{BET}) and pore size distribution were determined using Brunauer–Emmett–Teller (BET) theory and the Barrett—Joyner—Halenda (BJH) model, respectively.

Ammonia temperature-programmed desorption (NH_3-TPD) was performed on a Micromeritics Autochem 2920 instrument. In both experiments, the samples were dried for 0.5 h with He flow (50 mL·min^{-1}) at 573 K. For NH_3-TPD, an excess amount of $NH_{3(g)}$ was fed into the sample cell after the sample was cooled down to 393 K. The weakly adsorbed $NH_{3(g)}$ was then removed by continuously flowing He for 30 min. Subsequently, the temperature was ramped to 773 K (10 K·min^{-1}) and the desorption of ammonia was quantified by

a calibrated mass spectrometer using the mass 16 Da (the mass of the molecular ion of ammonia).

Diffuse-reflectance Fourier transform infrared spectroscopy with pyridine probe (Pyridine-DRIFTS) was performed on a PerkinElmer Frontier IR instrument. The physisorbed water was removed *in situ* by heating the samples to 423 K under reduced pressure (<10^{-2} mbar) for 3 h. A pyridine-helium mixture was then fed into sample cell at 323 K by flowing pure He (~50 mL·min^{-1}) into a round bottom flask containing cold pyridine and 4Å molecular sieve. After purging with He for 15 min, the DRIFTS spectra were then recorded at elevated temperatures under a continuous flow of pure He.

Powder x-ray diffraction (XRD) measurements were performed in a PANalytical Empyrean system (Theta-Theta, 240 mm) using Cu K-α as a radiation source. X-Ray Photoelectron Spectroscopy (XPS) measurements were carried out using a PHI VersaProbe II scanning XPS microprobe (Physical Instruments AG, Germany). Analysis was performed by using a monochromatic Al Kα X-ray source at a power of 24.8 W with a beam size of 100 μm. The spherical capacitor analyzer was set at a 45° take-off angle with respect to the sample surface. The pass energy was 46.95 eV yielding a full width at half maximum of 0.91 eV for the Ag 3d 5/2 peak.

Transmission electron microscope (TEM) images were obtained on a FEI Talos instrument with a 200 kV acceleration voltage. The samples were loaded on Lacey carbon grids. High-angle annular dark field scanning transmission electron microscopy (HAADF-STEM) images were obtained using an annular dark field detector to acquire images with atomic number contrast. Energy-Dispersive X-ray spectroscopy (EDX) was performed in the HAADF-STEM mode and analyzed using Bruker Esprit software.

^{1}H magic-angle spinning solid-state nuclear magnetic resonance (ssNMR) experiments were performed on a Bruker 400MHz spectrometer equipped with a 2.5 mm probe. A regular spin echo program with a spinning rate of 35 kHz was used to acquire the spectra. The samples were dried at 393 K under reduced pressure for 3 h and packed in the rotors in a glove box under inert atmosphere.

Material synthesis

HY-340 was pretreated by calcination at two different temperatures for 3 h. HY-340 calcined at 573 K is simply denoted as HY-340 whereas HY-340 calcined at 773 K is denoted as HY-340T. Silica spheres were synthesized by the Stöber method.[24] Typically, 3.8 mL of TEOS, 7.7 mL NH_3 (ca. 25%) and 18 mL of deionized water were mixed with 120 mL ethanol. The mixture was stirred and reacted at room temperature for 24 h. The product was centrifuged and

Journal Name

ARTICLE

washed with ethanol and then water. SBA-15 was synthesized based on a previously published method that was slightly modified.[25] Specifically, 2.8 g P-123 was dissolved in 104 g of 1.6 M HCl$_{(aq)}$ by vigorous stirring. 4 mL of TMOS was then slowly added and the resulting mixture was stirred for 24 h. Subsequently, the suspension was transferred into a Teflon lined stainless steel autoclave and heated at 110 °C for 24 h. After the hydrothermal treatment, the surfactant was removed by ethanol extraction using a standard Soxhlet apparatus for 24 h. Both silica substrates were calcined at 773 K for 5 h under a flow of synthetic air (ramping rate: 2 K·min^{-1}). Mesoporous niobia (m-Nb$_2$O$_5$) was synthesized following a reported method.[18] Briefly, 1 g P-123 was mixed with 10 g of ethanol. This solution was then mixed with 2 g of NbCl$_5$ while vigorous stirring was applied. The solvent of the resulting mixture was then slowly evaporated and the resulting solid was aged in air at 313 K for 2 days. After aging, the gel was calcined in a muffle furnace at 673 K for 5 h.

To synthetize overcoated samples, we applied a methodology similar to our previous work where we first calculated the quantity of Nb(OEt)$_5$ that was necessary to achieve single atomic monolayer coverage by dividing the S$_{BET}$ of substrate by the Van Der Waals projection area of Nb(OEt)$_5$ (0.765 nm^2, estimated by MarvinSketch)[23]. For 0.5 g SBA-15 (S$_{BET}$ = 750 m^2·g^{-1}), the monolayer amount of Nb(OEt)$_5$ (i.e. for synthesizing 1Nb$_2$O$_5$@SBA-15) was 0.8 mmol. As previously shown, we used a bidentate ligand (EAA) to chelate aluminum sec-butoxide in order to slow down the gelation rate of alumina for sol-gel overcoating.[23] Similarly, the precursor in this work was prepared by mixing Nb(OEt)$_5$ with 3 equivalent amount EAA under N$_2$ atmosphere. This led to a slower condensation rate and prevented uncontrolled Nb$_2$O$_5$ precipitation during sol-gel coating.[26] Subsequently, the mixture was diluted with ethanol and the final volume of the precursor was fixed to 10 mL. The resulting precursor solution was stirred at ambient temperature for 18 h. The general synthesis method for xNb$_2$O$_5$@SBA-15 was as follows: 0.5 g SBA-15 was dispersed in a mixture containing ethanol, water and NH$_{3(aq)}$. The quantities of water and ethanol in the suspension were proportional to the number of moles of injected Nb(OEt)$_5$. Specifically, the molar ratio of Nb(OEt)$_5$, water and ethanol was kept to 1:5:535. The volume of 25 wt% NH$_{3(sq)}$ in the suspension was fixed at 0.02 mL. The coating was initiated by injecting the aforementioned precursor solution into the suspension using an automatic syringe pump (KDS 100 legacy syringe pump) and the injection rate was set to 1.5 mL·min^{-1}. The suspension was vigorously stirred, soaked in an ice bath during the injection process and then kept at room temperature for 18 h after the injection was completed.

12Nb$_2$O$_5$@SiO$_2$ was synthesized using a similar protocol: 5 g Stöber silica was dispersed in a solution containing 50 mL ethanol, 0.04 mL NH$_3$ and 0.75 mL H$_2$O. A mixture of 1.6 mmol Nb(OEt)$_5$, 4.8 mmol EAA and 9 mL ethanol was then injected into the suspension at the rate of 1.5 mL·min^{-1}. The subsequent experimental conditions are the same as the procedure for xNb$_2$O$_5$@SBA-15. All the overcoated samples were thoroughly washed with ethanol and water and calcined at 773 K for 3 h to remove the remaining organic impurities.

Catalytic testing

Xylose dehydration was performed in an Alltech 10 mL thick-walled glass reactor. Typically, 75 mg xylose was dissolved in 2 mL H$_2$O and mixed with 3 mL toluene. 100 mg of catalyst was then loaded into the reactor and mechanically stirred (550 rpm) at 393 K for 5 h. The organic phase was analyzed by an Agilent Technologies 7890 A gas chromatography (GC) equipped with a flame ionization detector (FID) and a HP-5 column (50 m, 0.32 mm). The aqueous phase was analyzed by an Agilent Technologies 1260 infinity high performance liquid chromatography (HPLC) equipped with a refractive index detector, a UV-Vis detector and a Bio-Rad Aminex HPX-87H column. The chromatography was carried out with a flow rate of 0.6 mL·min^{-1} at 333 K using 5 mM H$_2$SO$_{4(aq)}$ as the mobile phase. The products were quantified using calibration curves produced by diluting analytical grade standards.

Friedel-Crafts alkylation was performed in an Alltech 10 mL thick-walled glass reactor. Typically, 50 mg catalyst was mixed with 1 mmol benzyl alcohol and 20 mmol anisole. The reaction proceeded by stirring the mixture (550 rpm) at 403 K for 3 h. The products were diluted with dioxane and analyzed by GC-FID. Benzyl alcohol was quantified using a calibration curve obtained produced by diluting a commercial standard while the three other products were quantified by using the effective carbon number method with decane as an internal standard.[27,28] The absence of significant mass transfer limitations for both reactions was confirmed by using the experiments with different stirring rates and by applying the Weisz–Prater criterion, which is shown in the supporting information.

Results and Discussion

Sol-gel based overcoating of Nb$_2$O$_5$ on silica substrate

An amount of Nb(OEt)$_5$ sufficient to produce 12 monolayers of the niobia overcoat was used to overcoat SiO$_2$ spheres in order to image the morphology of the deposited Nb$_2$O$_5$. A uniform Nb$_2$O$_5$ shell with a thickness of ~2 nm was formed on the sphere (Fig. 1a and b).

ARTICLE

Journal Name

The S_{BET} of SiO_2 slightly increased after coating (from 12 to 15 m²·g⁻¹), implying that the Nb_2O_5 shell was slightly porous. The image with higher magnification (Fig. 1b) shows that some nano-sized Nb_2O_5 clusters sporadically formed on the silica surface. This observation is in agreement with our previous simulation and experimental work which supported that the formation of metal oxide overcoats via solution sol-gel chemistry route proceed by an oligomer-deposition mechanism.[23,29] Such a mechanism could result in some porosity when niobia nanoparticles with different sizes aggregate and cover the surface and the larger niobia clusters might evolve from the larger sol particles.
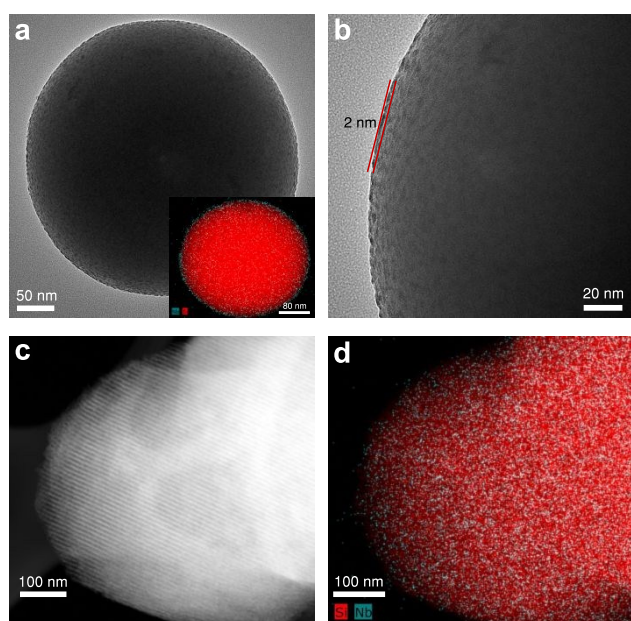

Fig. 1 TEM and STEM images of (a) $12Nb_2O_5@SiO_2$ with EDX mapping (inset), (b) $12Nb_2O_5@SiO_2$ with higher magnification, (c) $1Nb_2O_5@SBA-15$ under HAADF mode and (d) $1Nb_2O_5@SBA-15$ under HAADF mode with EDX mapping.

We further tried to overcoat SBA-15 as a post-modification strategy to synthesize mesoporous niobia with high surface area and an ordered pore structure. Due to the slower condensation kinetics of the chelated $Nb(OEt)_5$, a niobia overcoat can grow conformally inside the mesopores of SBA-15, as confirmed by STEM microscopy and EDX mapping (Fig. 1c and d). The morphology of SBA-15 did not significantly change with the increasing number of deposited Nb_2O_5 layers (Fig. S1 to S3). Small-angle XRD was then used to characterize the porous structures of overcoated SBA-15. Pristine SBA-15 displays three typical diffraction peaks that are the characteristics of *P6mm* hexagonal symmetry. The intensity of the diffraction peaks was reduced after overcoating but still fully present after 1 layer (Fig. 2a). The largest diffraction peak was maintained regardless of the number

of layers indicating that a regular pore structure was conserved. The disappearance of the smaller diffraction peaks with increasing layers could be attributed to the scattering of X-ray by the overcoat rather than pore degradation, which was further supported by physisorption (Fig. 2b) using the BJH model.[30] The overcoated samples still had a narrow pore size distributions and the pore volumes consistently decreased with increasing niobia loading. More importantly, the mean pore diameter reduced linearly with the number of Nb_2O_5 layers, implying a precise thickness control could be achieved (approximately 0.8 nm per layer, inset in Fig. 2b). Overcoating Nb_2O_5 onto SBA-15 was previously reported by either using ALD or sequential sol-gel grafting.[22,31] Comparing to these reported methods, our new wet-chemistry based approach has the advantages over both the ALD and grafting method. The presented coating procedure can be easily performed without a complicated ALD equipment or multiple grafting steps, yet is capable of achieving a reasonable degree of thickness control with nano-scale precision that is similar to ALD.
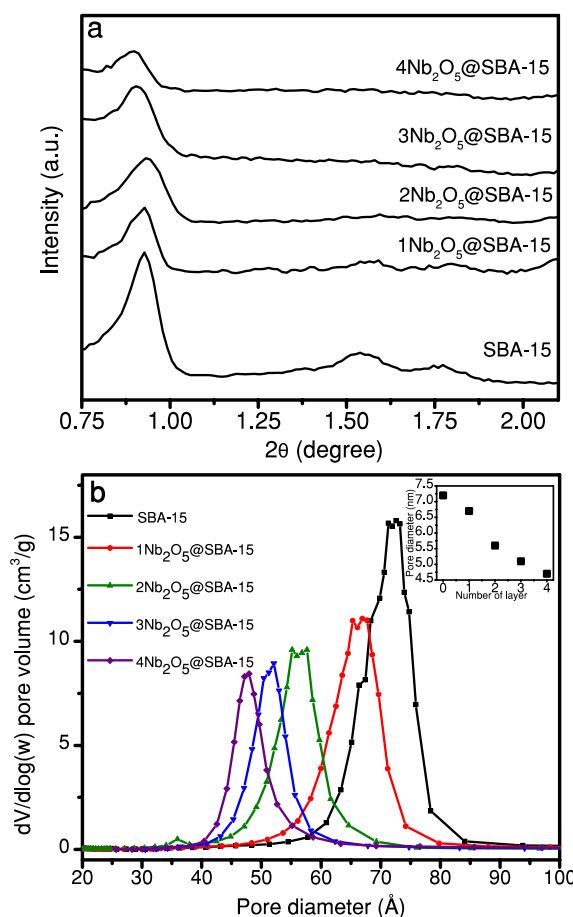

Fig. 2 (a) Small-angle XRD results of uncoated and overcoated SBA-15. The peaks in SBA-15 from small to large angle represent the 100, 110 and 200 diffractions (2D *P6mm* hexagonal symmetry).[32] (b) Pore size distributions of uncoated and overcoated SBA-15. The inset is the plot of the mean pore diameter versus the number of deposited niobia layers.

Structural and acid properties of Nb₂O₅@SBA-15 and bulk niobia

Because of the porous nature of our niobia overcoat, the silica functionality (e.g. silanol group) might remain accessible at the surface. Therefore, we performed XPS to investigate the surface compositions of Nb_2O_5@SBA-15 (Fig. 3). The O 1s XPS results of SBA-15 and four overcoated samples showed a clear transition from a pure Si-O signal to a Nb-O signal. Although a very weak Si signal could still be detected (Nb/Si = 9.4, Table 1), we concluded that $4Nb_2O_5$@SBA-15 showed nearly full Nb_2O_5 coverage on the surface according to the O 1s data. The signal of Nb 3d, on the other hand, provided information of the niobium environment. Both bulk niobia and the overcoated samples showed typical doublet peaks, which is known to be due to the spin-orbit coupling of the Nb 3d orbitals. The binding energy of the doublet increases with a higher oxidation state of the niobium.[33,34] The Nb 3d signals of the $4Nb_2O_5$@SBA-15 and HY-340 almost overlap while the signals of $m-Nb_2O_5$ have lower binding energies, indicating there was an increasing Nb^{4+} character in $m-Nb_2O_5$. According to the model proposed by Kreissl et. al, Nb^{4+} exists as an oxygen-deficient five-coordinated center in the Nb_2O_5 network, which is structurally distinct from the typical octahedral NbO_6 unit. Accordingly, the Nb_2O_5 overcoat and HY-340 were likely comprised of mainly NbO_6 units but $m-Nb_2O_5$ had more pyramidal NbO_5 units on the surface.

Acid catalysis is an important application for niobia. To evaluate this aspect of the overcoated material, the total acid sites of Nb_2O_5@SBA-15 and bulk niobia catalysts were quantified by NH_3-TPD (Table 1). $4Nb_2O_5$@SBA-15 had the largest number of total acid sites per weight among all samples since its S_{BET} outnumbered all bulk niobia samples. Overall, HY-340 had the largest number of total acid sites per surface area among all materials. However, the number of acid sites were drastically reduced when being calcined at 773 K (HY-340T). In this case, HY-340 underwent structural transformation from an amorphous to pseudo-hexagonal phase during the thermal treatment (Fig. S4), which caused the loss of acid sites as previously reported.[15,16] The as-synthesized $m-Nb_2O_5$ had an intrinsic pseudo-hexagonal structure and a similarly low number of acid sites as the thermally treated HY-340T. Interestingly, all overcoated Nb_2O_5@SBA-15 retained their amorphous structure and large number of acid sites even after a high temperature thermal treatment (773 K), which was required to effectively remove the remaining precursor impurities during the synthesis. We attributed the limited crystallization to the presence of Si-O-Nb bonds between the overcoat and the support. The amorphous phase was likely stabilized by the

presence of these strong bonds. A similar observation was also previously reported for ZrO_2 overcoats on SBA-15.[30]
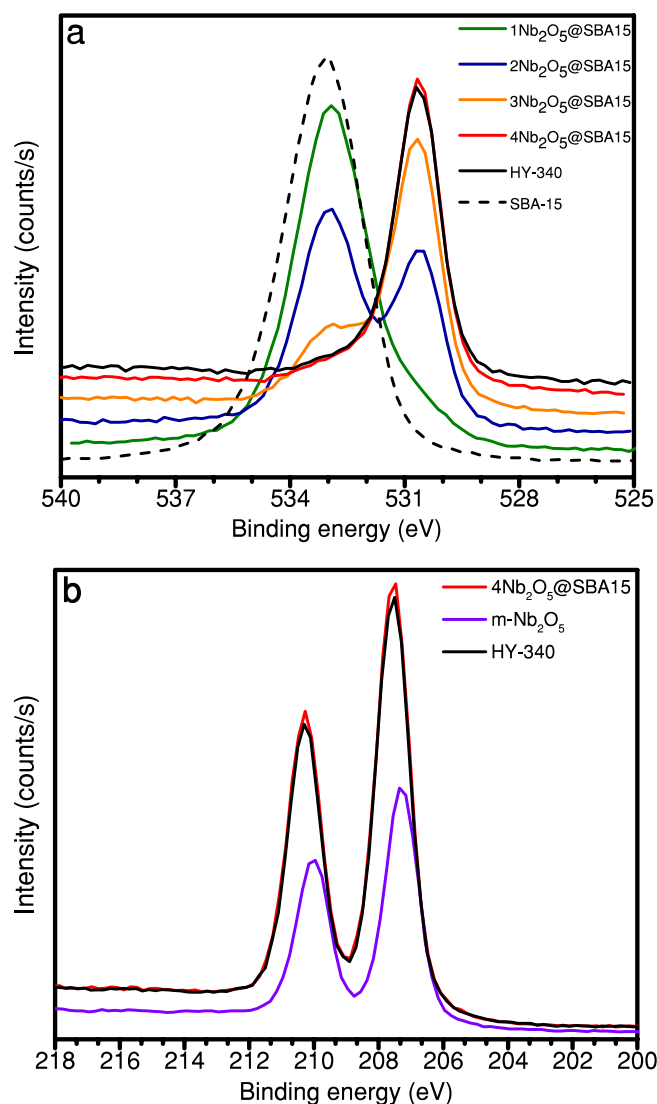
Fig. 3 (a) O 1s XPS results for SBA-15, overcoated SBA-15 and HY-340 (b) Nb 3d results for $4Nb_2O_5$@SBA-15, $m-Nb_2O_5$ and HY-340.

The total number of acid sites per surface area of Nb_2O_5@SBA-15 was considerably lower than both types of bulk niobia (Table 1), which could be explained by incomplete Nb_2O_5 coverage in the micropores of SBA-15. Indeed, silanol groups could still be observed by XPS, DRIFTS (Fig. S5a) and ^1H ssNMR (Fig. S6) for $4Nb_2O_5$@SBA-15. We hypothesize that $Nb(OEt)_5$ is probably too bulky to effectively diffuse into the micropores of SBA-15 and react, thus leaving some unreacted Si-OH at the surface. This phenomenon was also observed when ALD was used to overcoat Nb_2O_5 onto SBA-15.[22] Since the micropores were not completely filled by Nb_2O_5, they

contributed to the surface area without adding acid sites, thus lowering the acid site density for overcoated SBA-15. Furthermore, we quantified the number of Brønsted acid sites of bulk and overcoated niobia catalysts using NH_3-TPD to quantify the total number of sites present and DRIFTS-pyridine (Fig. S7) to measure the ratio of Brønsted to Lewis acid sites using a previously reported ratio of extinction coefficients. [35] Specifically, the ratio of the two acid types were estimated using the integrated band area of the peaks at 1445 cm^{-1} and 1535 cm^{-1}, which were assigned to the pyridine adsorbed on Lewis and Brønsted acid sites, respectively. The catalysts with the highest Brønsted/Lewis acid site (B/L) ratio were, in order, HY-340 > m-Nb_2O_5 > $4Nb_2O_5$@SBA-15. Lewis acid sites have been hypothesized to originate from niobium centers with lower coordination numbers and Brønsted acid sites are contributed by the Nb-OH groups associated to NbO_6 units. [36] Therefore, the acid characterization results of HY-340 and m-Nb_2O_5 agreed with the structural features that were suggested by the XPS experiments. Namely that the niobium in HY-340 had a higher coordination number than the niobium in m-Nb_2O_5. However, XPS data could have led us to believe that $4Nb_2O_5$@SBA-15 and HY-340 would have had similar B/L ratio because these analyses suggested that their surfaces were mainly composed of NbO_6 units. Instead, the much smaller B/L ratio (1/3) of $4Nb_2O_5$@SBA-15 could have resulted from the self-condensation of Nb-OH group during the calcination at 773 K, which could have proceeded by a similar mechanism as what occurs on amorphous silica surfaces. [37,38]

Catalytic behavior of mesoporous Nb_2O_5 and bulk catalysts

To investigate the catalytic activity of overcoated SBA-15 as a solid acid, we used two typical acid-catalyzed reactions as probes: xylose dehydration and Friedel-Crafts alkylation. Dehydrating xylose to form furfural catalyzed by Nb_2O_5 has been widely investigated. [8,10,13] Xylose is believed to first isomerize into xylulose over a Lewis acid site and further dehydrate to furfural, which is catalyzed by Brønsted acid sites. [39,40] The selectivity of furfural is highly dependent on the ratio of Brønsted/Lewis acid sites in the catalyst. [13,41] We performed xylose dehydration in a standard biphasic system (water/toluene) in order to continuously extract furfural and avoid its degradation by further rehydration and condensation reactions (e.g. levulinic acid and humin formation). $4Nb_2O_5$@SBA-15 showed the highest conversion (91%) among all overcoated samples (Fig. 4). However, the conversion of HY-340 was higher (96%) than that of $4Nb_2O_5$@SBA-15 (91%), even though it had slightly fewer acid sites (Table 1).

Despite the high conversion, the furfural selectivity of HY-340 was much lower (44%) than that of the overcoated catalyst, which was likely due to the aforementioned side reactions that occurred at nearly full conversion. [42] A higher selectivity could be obtained (50%) with a shorter reaction time (3 h), but HY-340 was still less selective to furfural than other catalysts. Moreover, HY-340 calcined at 773 K also showed low selectivity towards furfural. Therefore, we suggested that the predominant Brønsted acidity (B/L ratio > 5) in HY-340 could favour rehydration and condensation reactions thus lowering the selectivity towards furfural.

Table 1. Characterization data of overcoated and bulk niobia catalysts

	S_{BET} (m^2/g)	Nb/Si ratio[a]	Total acid sites[b]		Brønsted acid sites[c]	Lewis acid sites[d]	Structure[e]
			μmol g^{-1}	μmol m^{-2}	μmol g^{-1}	μmol g^{-1}	
SBA-15	750	-	-	-	-	-	amorphous
$1Nb_2O_5$@SBA15	558	0.12	228	0.41	-	-	amorphous
$2Nb_2O_5$@SBA15	521	0.63	210	0.40	-	-	amorphous
$3Nb_2O_5$@SBA15	419	2.3	237	0.56	-	-	amorphous
$4Nb_2O_5$@SBA15	471	9.4	296	0.63	76	220	amorphous
m-Nb_2O_5	91	-	139	1.53	79	60	TT-phase
HY-340	72	-	278	3.86	238	40	amorphous
HY-340T	67	-	97	1.45	-	-	TT-phase

[a] Determined by XPS.
[b] Determined by NH_3-TPD.
[c] Determined by pyridine-DRIFTS
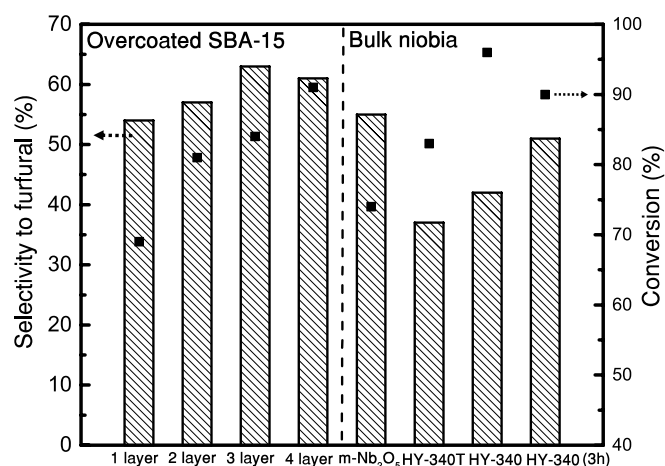[e] Determined by XRD

Fig. 4 Xylose dehydration using different niobia catalysts. Points represent conversion and bars represent furfural selectivity.

The increasing conversion with each deposition cycle can likely be explained by the increasing extent of niobia coverage on the surface, which led to an increasing number of acid sites (especially Brønsted acid sites) and increased number of adsorption sites for xylose. At the same time, selectivity did not increase as rapidly because it likely depended more on the ratio of Brønsted acid and Lewis acid sites rather than the total number of acid sites. This ratio likely remained fairly constant with the increasing coverage, so the selectivity did not vary as much as the conversion increased. Interestingly, we observed that 3Nb2O5@SBA-15 and 4Nb2O5@SBA-15 had slightly increased selectivities to furfural. This result might be related to limited xylose degradation reactions that occur in the solution. Increasing the conversion of xylose might lower the extents of those side reactions and hence slightly increase the selectivity. The highest yield of furfural (56% at 3h) was obtained with 4Nb2O5@SBA-15, and we attributed the high yield to its balanced B/L ratio, which maximized conversion while limiting byproduct formation.

We further studied the activities of $4Nb_2O_5$@SBA-15 and other bulk niobia materials during Friedel-Crafts alkylation, which is an important reaction for arene substitution. Friedel-Crafts alkylation is typically catalyzed by Lewis acid sites but requires Brønsted acid sites when the alkylating reagent is an alcohol.[21,43,44] The use of a solid acid and an alcohol alkylation agent is considered more environmentally friendly than traditional homogeneous Lewis acids (e.g. $AlCl_3$). We studied the benzylation of anisole using benzyl alcohol because such benzyl benzene derived molecules are considered industrially valuable.[45,46] Specifically, two structural isomers (para- and ortho-

benzyl anisole) and benzyl ether (side product) were obtained in this reaction. The four tested catalysts showed identical product distributions and similar selectivity to benzylated products (Fig. 5a).
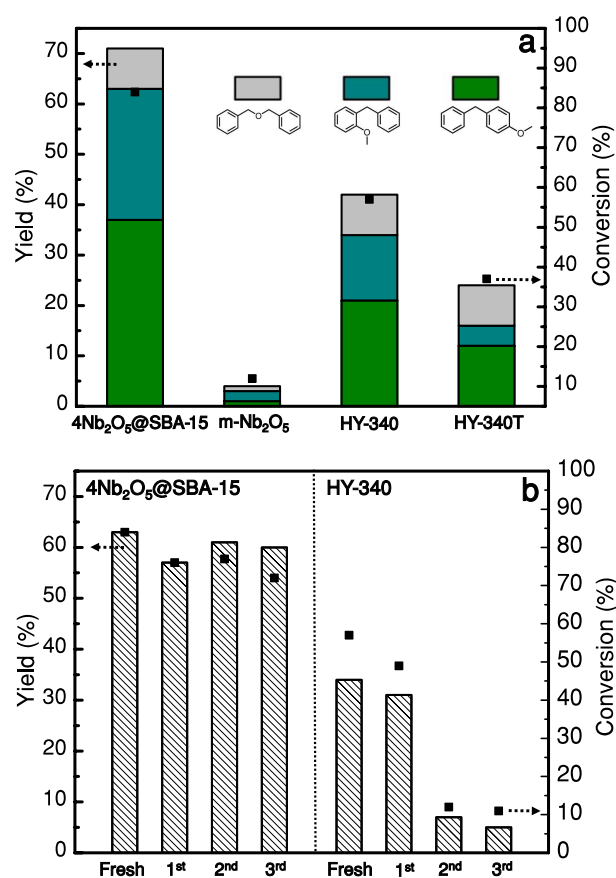

Fig. 5 (a) Yield and distribution of products in the Friedel-Crafts alkylation catalyzed by different forms of niobia. (b) Catalyst stability test of $4Nb_2O_5$@SBA-15 and HY-340 after regenerations. The yield is the sum of the two benzylated products.

However, the differences in activity were distinct from that of xylose dehydration. Using $4Nb_2O_5$@SBA-15 led to the highest conversion (84%) and yield of benzyl anisole (63%, including two isomers) at 3 h. In contrast, HY-340, the catalyst with the largest number of Brønsted acid sites, led to only 57% conversion. The lowest conversion was again obtained over $m-Nb_2O_5$. HY-340T showed a reduced activity (37% of conversion) compared to HY-340, presumably because of the loss of its acid sites during phase transformation. We also noticed that the catalysts' color changed when the conversion neared 100% (Fig. S8). We repeated the reaction using spent $4Nb_2O_5$@SBA-15 and a lower conversion was obtained (45%), which can be ascribed to the formation of some condensed byproducts that blocked acid sites. Therefore, the spent

4Nb$_2$O$_5$@SBA-15 and HY-340 were regenerated by calcination at 773 K for 1 h to remove deposits and the activities of regenerated catalysts were studied (Fig. 5b). The conversion of 4Nb$_2$O$_5$@SBA-15 at 3 h slightly decreased after first regeneration but it remained stable in the second and third catalytic runs. In contrast, the activity of HY-340 dropped after the second regeneration. Further XRD analyses showed that the structure of the regenerated HY-340 became pseudo-hexagonal while 4Nb$_2$O$_5$@SBA-15 remained amorphous (Fig. S4b). These results further suggested that the acid sites of 4Nb$_2$O$_5$@SBA-15 had an exceptional resistance against thermal treatment, which could be advantageous in industrial processes where catalyst regenerations are required.

As previously mentioned, the Brønsted acid sites are considered to be the active site in this Friedel-Crafts alkylation. Therefore, we determined the turnover frequency (TOF) of 4Nb$_2$O$_5$@SBA-15, HY-340 and m-Nb$_2$O$_5$ by dividing their extrapolated initial reaction rates by the numbers of Brønsted acid sites (Fig. 6). Interestingly, the TOF of 4Nb$_2$O$_5$@SBA-15 (0.06 s^{-1}) was 6 times higher than the TOF of HY-340 (0.009 s^{-1}) while m-Nb$_2$O$_5$ displayed a TOF that was nearly one order of magnitude lower than these two catalysts (TOF = 0.001 s^{-1}). We hypothesized that the variation in activity may result from the difference in acidity strength between these various catalysts. DRIFTS-pyridine was then conducted and the spectra were collected at 573 K (Fig. 6d) to study the presence of strongly chemisorbed pyridine. The adsorbed pyridine species and their corresponding acid type were assigned according to previous reports in the literature.[47,48] We observed only two peaks that corresponded to Lewis acid sites on m-Nb$_2$O$_5$, whereas pyridines adsorbing on Brønsted acid sites were found on both 4Nb$_2$O$_5$@SBA-15 and HY-340. This result substantiated that the acidity of m-Nb$_2$O$_5$ was weaker, thus leading to a significantly lower TOF for Friedel-Crafts alkylation. In contrast, the peak at 1520 cm^{-1}, which was assigned to Brønsted acid sites, was measured even at this higher temperature for both HY-340 and 4Nb$_2$O$_5$@SBA-15, which was indicative of strong Brønsted acidity . We further examined NH$_3$-TPD data (Fig. S9) and found that HY-340 had an extra desorption band at 653 K, which was not detected for 4Nb$_2$O$_5$@SBA-15. This result implied that HY-340 was more acidic, which led us to conclude that acid strength alone could not account for the higher activity of 4Nb$_2$O$_5$@SBA-15.
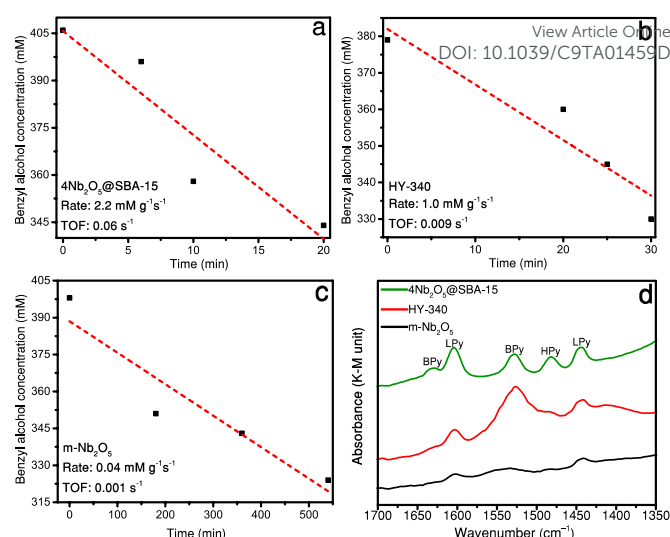

Fig. 6 Kinetic study of Friedel-Crafts alkylation. Initial rate determination and TOF calculation for (a) 4Nb$_2$O$_5$@SBA-15, (b) HY-340 and (c) m-Nb$_2$O$_5$. The initial reaction rates were determined by the extrapolation to time zero of the least squares fit of reactant concentration versus reaction time at conversions below 20%. The reaction conditions were the same as what is shown in the experimental section except the amount of catalyst added for 4Nb$_2$O$_5$@SBA-15 and HY-340, which were reduced to 25 mg to maintain low conversion. (d) DRIFTS-Pyridine results. BPy, LPy and HPy denote pyridine adsorbing on Brønsted acid sites, pyridine adsorbing on Lewis acid site and H-bonded pyridine, respectively. The presented data were smoothed using the adjacent-averaging method with a 15 point window.

In order to understand the discrepancy in acid strength and catalytic activity between HY-340 and 4Nb$_2$O$_5$@SBA-15, we ran ^{1}H ssNMR measurements to characterize the surface hydroxyl groups at the atomic level (Fig. 7). HY-340 showed a broad peak centered at 5.7 ppm and another narrower peak with much lower intensity at 2.7 ppm. In comparison, 4Nb$_2$O$_5$@SBA-15 showed a broad peak centered at 4.9 ppm and two partially overlapping peaks at 2.4 ppm and 2.2 ppm. The peak at 2.4 ppm was assigned to Nb–OH and the peak 2.2 ppm was assigned to the remaining silanol groups from the micropores of SBA-15 support (^{1}H ssNMR spectra of pure SBA-15 is shown in Fig. S6, confirming the silanol group assignment). Consequently, both niobia catalysts showed two Nb–OH species but the ratio of these two hydroxyl groups seemed to be different. Takagaki et al.[21,49,50] have performed detailed studies on niobia and have assigned the broader peak to a hydrogen bonded proton and the narrower peak to a terminal Nb–OH. Takagaki et al. also suggested that the Nb–OH groups with hydrogen bonding, which lead to the broad peak at higher ppms, had a stronger acidity. The high proportion of hydrogen bonded Nb–OH on HY-340 could have led to its stronger acidity, which is in a good

ARTICLE

agreement with our NH₃-TPD analyses. Compared to HY-340, 4Nb₂O₅@SBA-15 had more isolated Nb–OH groups, which were less acidic than the hydrogen-bonded hydroxyl groups. We attributed this result to the structural difference between 4Nb₂O₅@SBA-15 and HY-340 and the hypothesized models are schematized (Fig. 7). HY-340 is known to be a mixture of nanoparticles with different sizes and hydrogen bonds can form within their interlayers. Furthermore, IPA chemisorption indicated that HY-340 had the highest density of Brønsted acid sites, which originated from the Nb–OH groups on the surface. This high density of the surface Nb–OH groups likely further promoted the hydrogen bond formation. In contrast, the niobia on 4Nb₂O₅@SBA-15 has a two dimensional structure because it was deposited as a thin film inside the pores of SBA-15. This nanostructure likely led the niobia to have a longer distance between Nb₂O₅ surfaces, which disfavoured hydrogen bond formation and increases the presence of exposed isolated Nb-OH groups. We propose that the high activity of 4Nb₂O₅@SBA-15 in Friedel-Crafts alkylation was due to its unique nanostructure and surface characteristics, which involves these isolated Nb-OH groups. The relatively sparse Nb-OH groups in the absence of hydrogen bonding could have lead anisole and benzyl alcohol to adsorb and react more easily compared to the case where a hydrogen bond network is formed, which could be unfavorable to the adsorption of such hydrophobic substrates. Our findings reveal that strong acidity does not guarantee activity during acid catalysis. An acid catalyst with the well-tailored nanostructure could lead to a higher catalytic performance even though it had slightly fewer and weaker acid sites.
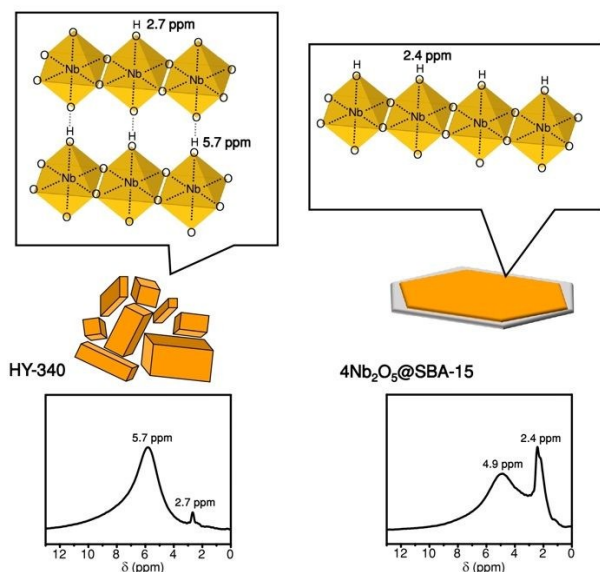

Fig. 7 ¹H ssNMR spectra and associated proposed schematic structure of HY-340 and niobia overcoated on silica (4Nb₂O₅@SBA-15).

Conclusions

By properly controlling the sol-gel kinetics of Nb(OEt)₅, a post synthesis strategy was developed for synthesizing a SBA-15 type mesoporous niobia with high surface area and narrow pore size distribution. This niobic acid exhibits superior catalytic activity in two probe reactions, namely xylose dehydration and Friedel-Crafts alkylation. The balanced ratio of Brønsted and Lewis acid sites on Nb₂O₅@SBA-15 resulted in a higher selectivity towards furfural compared to bulk niobia catalysts. On the other hand, the tailored nanostructure of overcoated catalyst restrained the formation of interlayer hydrogen bonds, which appeared to be favourable for Friedel-Crafts alkylation with hydrophobic reactants. This structural advantage led to a higher activity despite its weaker acidity. Importantly, the overcoating strategy also imparted a higher thermal stability to Nb₂O₅. The acid sites could resist high temperature thermal treatments (773 K) which led to its activity being retained after catalyst regenerations. In contrast, these high temperatures caused phase transformations in HY-340 and the mesoporous niobia synthesized using traditional template assisted methods, which irreversibly reduced the number of acid sites. Overall, not only did kinetically controlled overcoating provide an easy method for producing high surface area niobia catalysts with a controlled mesoporous structure, but it also led to unique structural stability and properties. Both phenomena, which were observed during different probe reactions, emphasize the importance of localized material structure in catalysis and could provide new insights and routes for the rational design of solid acid catalysts.

Conflicts of interest

There are no conflicts to declare.

Acknowledgements

Notes and references

1   S. Park, S. Park, S. Lee, H. W. Kim and C. Lee, *Sensors and Actuators B: Chemical*, 2014, **202**, 840–845.

2   W. Luo, Y. Li, J. Dong, J. Wei, J. Xu, Y. Deng and D. Zhao, *Angewandte Chemie International Edition*, 2013, **52**, 10505–10510.

3   C. Opris, B. Cojocaru, N. Gheorghe, M. Tudorache, S. M. Coman, V. I. Parvulescu, B. Duraki, F. Krumeich and J. A. van Bokhoven, *ACS Catal.*, 2017, **7**, 3257–3267.

4   Q. Xia and Y. Wang, in *Nanoporous Catalysts for Biomass Conversion*, John Wiley & Sons, Ltd, 2017, pp. 253–281.

5   Y. Shao, Q. Xia, L. Dong, X. Liu, X. Han, S. F. Parker, Y. Cheng, L. L. Daemen, A. J. Ramirez-Cuesta, S. Yang and Y. Wang, *Nature Communications*, 2017, **8**, 16104.

6   N. Özer, T. Barreto, T. Büyüklimanli and C. M. Lampert, *Solar Energy Materials and Solar Cells*, 1995, **36**, 433–443.

7   S. Furukawa, T. Shishido, K. Teramura and T. Tanaka, *ACS Catal.*, 2012, **2**, 175–179.

8   C. García-Sancho, I. Agirrezabal-Telleria, M. B. Güemez and P. Maireles-Torres, *Applied Catalysis B: Environmental*, 2014, **152**–**153**, 1–10.

9   G. S. Foo, D. Wei, D. S. Sholl and C. Sievers, *ACS Catal.*, 2014, **4**, 3180–3192.

10 C. García-Sancho, I. Sádaba, R. Moreno-Tost, J. Mérida-Robles, J. Santamaría-González, M. López-Granados and P. Maireles-Torres, *ChemSusChem*, **6**, 635–642.

11 W. Fan, Q. Zhang, W. Deng and Y. Wang, *Chemistry of Materials*, 2013, **25**, 3277–3287.

12 M. Moraes, W. de. S. F. Pinto, W. A. Gonzalez, L. M. P. M. Carmo, N. M. R. Pastura and E. R. Lachter, *Applied Catalysis A: General*, 1996, **138**, L7–L12.

13 N. K. Gupta, A. Fukuoka and K. Nakajima, *ACS Catal.*, 2017, **7**, 2430–2436.

14 H. T. Kreissl, K. Nakagawa, Y.-K. Peng, Y. Koito, J. Zheng and S. C. E. Tsang, *Journal of Catalysis*, 2016, **338**, 329–339.

15 T. Murayama, J. Chen, J. Hirata, K. Matsumoto and W. Ueda, *Catal. Sci. Technol.*, 2014, **4**, 4250–4257.

16 H. T. Kreissl, M. M. J. Li, Y.-K. Peng, K. Nakagawa, T. J. N. Hooper, J. V. Hanna, A. Shepherd, T.-S. Wu, Y.-L. Soo and S. C. E. Tsang, *J. Am. Chem. Soc.*, 2017, **139**, 12670–12680.

17 K. Nakajima, J. Hirata, M. Kim, N. K. Gupta, T. Murayama, A. Yoshida, N. Hiyoshi, A. Fukuoka and W. Ueda, *ACS Catal.*, 2018, **8**, 283–290.

18 P. Yang, D. Zhao, D. I. Margolese, B. F. Chmelka and G. D. Stucky, *Nature*, 1998, **396**, 152–155.

19 K. Nakajima, T. Fukui, H. Kato, M. Kitano, J. N. Kondo, S. Hayashi and M. Hara, *Chem. Mater.*, 2010, **22**, 3332–3339.

20 P. Yang, D. Zhao, D. I. Margolese, B. F. Chmelka and G. D. Stucky, *Chem. Mater.*, 1999, **11**, 2813–2826.

21 A. Takagaki, D. Lu, J. N. Kondo, M. Hara, S. Hayashi and K. Domen, *Chem. Mater.*, 2005, **17**, 2487–2489.

22 Y. J. Pagán-Torres, J. M. R. Gallo, D. Wang, H. N. Pham, J. A. Libera, C. L. Marshall, J. W. Elam, A. K. Datye and J. A. Dumesic, *ACS Catal.*, 2011, **1**, 1234–1245.

23 Y.-P. Du, F. Héroguel and J. S. Luterbacher, *Small*, 2018, **14**, 1801733.

24 W. Stöber, A. Fink and E. Bohn, *Journal of Colloid and Interface Science*, 1968, **26**, 62–69.

25 A. Galarneau, H. Cambon, F. D. Renzo, R. Ryoo, M. Choi and F. Fajula, *New J. Chem.*, 2003, **27**, 73–79.

26 I. Yoshinaga, N. Yamada and S. Katayama, *J Sol-Gel Sci Technol*, 2005, **35**, 21–26.

27 J. T. Scanlon and D. E. Willis, *J Chromatogr Sci*, 1985, **23**, 333–340.

28 L. Shuai, M. T. Amiri, Y. M. Questell-Santiago, F. Héroguel, Y. Li, H. Kim, R. Meilan, C. Chapple, J. Ralph and J. S. Luterbacher, *Science*, 2016, **354**, 329–333.

29 K. S. Brown, C. Saggese, B. P. Le Monnier, F. Héroguel and J. S. Luterbacher, *J. Phys. Chem. C*, 2018, **122**, 6713–6720.

30 C. K. Krishnan, T. Hayashi and M. Ogura, *Adv. Mater.*, 2008, **20**, 2131–2136.

31 J. N. Kondo, Y. Hiyoshi, R. Osuga, A. Ishikawa, Y.-H. Wang and T. Yokoi, *Microporous and Mesoporous Materials*, 2018, **262**, 191–198.

32 D. Zhao, J. Feng, Q. Huo, N. Melosh, G. H. Fredrickson, B. F. Chmelka and G. D. Stucky, *Science*, 1998, **279**, 548–552.

33 M. Grundner and J. Halbritter, *Journal of Applied Physics*, 1980, **51**, 397–405.

34 Z. P. Hu, Y. P. Li, M. R. Ji and J. X. Wu, *Solid State Communications*, 1989, **71**, 849–852.

35 A. Platon and W. J. Thomson, *Ind. Eng. Chem. Res.*, 2003, **42**, 5988–5992.

36 K. Nakajima, Y. Baba, R. Noma, M. Kitano, J. N. Kondo, S. Hayashi and M. Hara, *J. Am. Chem. Soc.*, 2011, **133**, 4224–4227.

37 L. T. Zhuravlev, *Colloids and Surfaces A: Physicochemical and Engineering Aspects*, 2000, **173**, 1–38.

38 F. Rascón, R. Wischert and C. Copéret, *Chemical Science*, 2011, **2**, 1449–1456.

39 V. Choudhary, S. I. Sandler and D. G. Vlachos, *ACS Catal.*, 2012, **2**, 2022–2028.

40 V. Choudhary, A. B. Pinar, S. I. Sandler, D. G. Vlachos and R. F. Lobo, *ACS Catal.*, 2011, **1**, 1724–1728.

41 R. Weingarten, G. A. Tompsett, W. C. Conner and G. W. Huber, *Journal of Catalysis*, 2011, **279**, 174–182.

42 E. I. Gürbüz, J. M. R. Gallo, D. M. Alonso, S. G. Wettstein, W. Y. Lim and J. A. Dumesic, *Angewandte Chemie International Edition*, 2013, **52**, 1270–1274.

43 E. Wada, M. Kitano, K. Nakajima and M. Hara, *J. Mater. Chem. A*, 2013, **1**, 12768–12774.

44 N. Narender, K. V. V. K. Mohan, S. J. Kulkarni and I. A. K. Reddy, *Catalysis Communications*, 2006, **7**, 583–588.

45 V. V. Bokade and G. D. Yadav, *Journal of Natural Gas Chemistry*, 2007, **16**, 186–192.

46 B. M. Khadilkar and S. D. Borkar, *Journal of Chemical Technology & Biotechnology*, 1998, **71**, 209–212.

47 J. Datka, A. M. Turek, J. M. Jehng and I. E. Wachs, *Journal of Catalysis*, 1992, **135**, 186–199.

48 M. N. Rashed, S. M. A. H. Siddiki, M. A. Ali, S. K. Moromi, A. S. Touchy, K. Kon, T. Toyao and K. Shimizu, *Green Chemistry*, 2017, **19**, 3238–3242.

49 A. Takagaki, M. Sugisawa, D. Lu, J. N. Kondo, M. Hara, K. Domen and S. Hayashi, *J. Am. Chem. Soc.*, 2003, **125**, 5479–5485.

50 A. Takagaki, C. Tagusagawa, S. Hayashi, M. Hara and K. Domen, *Energy Environ. Sci.*, 2010, **3**, 82–93.